THE JOURNAL OF PHYSICAL CHEMISTRY C
A JOURNAL OF THE AMERICAN CHEMICAL SOCIETY

pubs.acs.org/JPCC

Article

Effect of Phase Transition on the Thermal Transport in Isoreticular DUT Materials

Penghua Ying, Jin Zhang,* and Zheng Zhong*

Cite This: J. Phys. Chem. C 2021, 125, 12991−13001

Read Online

ACCESS | Metrics & More | Article Recommendations | Supporting Information

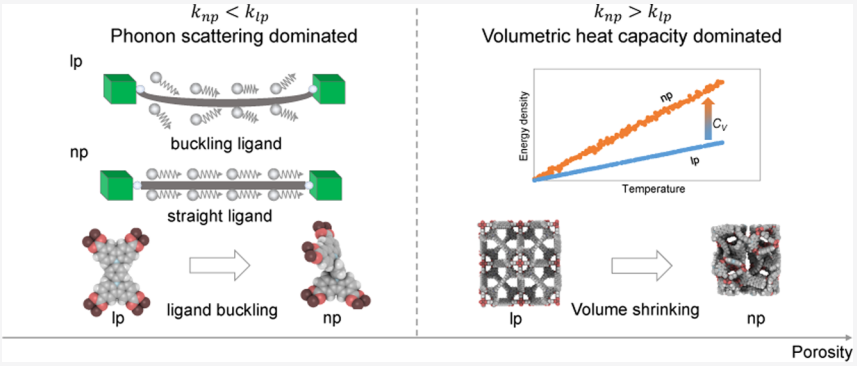

ABSTRACT: Soft porous crystals (SPCs) or flexible metal−organic frameworks have great potential applications in gas storage and separation, in which SPCs can undergo phase transition due to external stimuli. Thus, understanding the effect of phase transition on the thermal transport in SPCs becomes extremely crucial because the latent heat generated in aforementioned applications is needed to be effectively removed. In this paper, taking the isorecticular DUT series as an example, the thermal transport property of SPCs during the phase transition from a large pore (lp) phase to a narrow pore (np) phase is comprehensively investigated by molecular dynamics simulations together with the Gree−Kubo method. According to our calculations, all DUT structures exhibit an ultralow thermal conductivity smaller than 0.2 W $m^{-1}K^{-1}$. In addition, we find that the effect of phase transition on the thermal transport property of different DUT materials considered here strongly depends on their porosities. As for DUT-48, its lp phase has a thermal conductivity larger than that of its np phase. However, in other DUT materials, i.e, DUT-47, DUT-49, DUT-50, and DUT-151, the thermal transport property of their lp phase is found to be weaker than that of their np phase. This complicated effect of phase transition on the thermal transport in SPCs can be explained by a porosity-dominated competition mechanism between the increased volumetric heat capacity and the aggravated phonon scattering during the phase transition process.

1. INTRODUCTION

Soft porous crystals (SPCs), coined by Kitagawa and colleagues in 2009,[1] refer to the flexible metal−organic frameworks (MOFs) or porous coordination polymers that own bistable or multistable phases with long-range crystal order.[1−5] The different phases of SPCs can switch to each other due to various external physical and chemical stimuli such as mechanical pressure, gas adsorption, temperature, electric fields, and light.[4,6] The stepwise expansion or contraction is observed in SPCs during the structural transition between large pore (lp) and narrow pore (np) phases. Other terms have also been used to describe the SPCs processing this dynamic behavior, which includes flexible frameworks,[2] stimuli-responsive materials,[4] and nanoscale metamaterials.[7] When compared with the rigid adsorbents, this dynamic behavior of SPCs makes them promising materials for new applications in gas storage and separation.[8−10] A very recent example among these applications is the novel negative gas adsorption (NGA) phenomenon of DUT-49,[11] in which a drop in the amount of adsorbed particles is observed with increasing vapor pressure. On the basis of reticular synthesis,[12] Krause and colleagues proposed a general network architecture design criterion for the NGA transition in isoreticular DUT materials,[13,14] among which DUT-50[13] and DUT-160[14] are found to exhibit an NGA behavior similar to that of DUT-49.[11] Several thermodynamic models have been developed to unravel the conditions determining the NGA in SPCs.[15−17] In our recent work,[18] the influence of phase transition on the mechanical properties of isoreticular DUT series has been

Received: March 28, 2021
Revised: May 22, 2021
Published: June 8, 2021

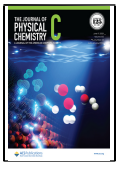

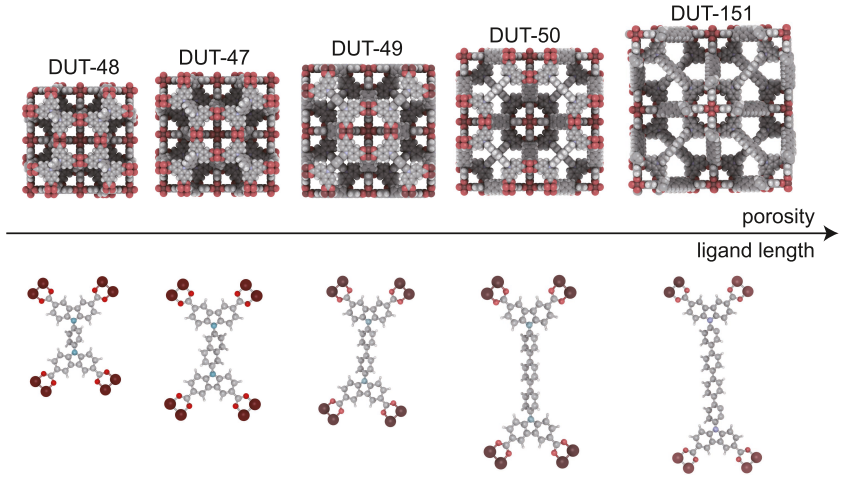

Figure 1. Atomic structures of isoreticular DUT materials. Cu, O, C, N, and H atoms are shown in brown, red, gray, cyan, and white colors, respectively.

comprehensively investigated by molecular dynamics (MD) simulations together with continuum mechanical models.

In spite of the fact that MOFs possess many unique properties, the thermal conductivity of MOFs is usually extremely low, which is typically smaller than 2 W $m^{-1}K^{-1}$ at room temperature[19−21] due to their ultraporous structures[22] and weak coordination bonds.[23] The property of ultralow thermal conductivity is recognized as the bottleneck of MOFs in energy-related applications such as adsorbent-based fuel tanks for methane- or hydrogen-powered vehicles.[24] Hence, it is crucial to obtain a more fundamental understanding of the nature and mechanism of the thermal transport in SPCs, which will facilitate their applications in practical industrial adsorbents. However, compared with the gas adsorption property, the study of the thermal transport in SPCs is still in its very early stage. To date, only the thermal conductivity of some conventional SPCs such as MOF-5,[23−26] ZIF-8,[27−32] and HKUST-1[21,33,34] has been investigated in detail by experimental or computational approaches, while the thermal transport properties of the aforementioned DUT series still remain unknown. In addition, the existing studies mainly focus on the influence of gas and water adsorption,[29,34] framework architecture,[24,28,35−38] defects,[33] and physical environment including pressure[18] and temperature[20] on the thermal conductivity of SPCs; little attention has been paid to the evolution of the thermal transport properties of SPCs during their dynamic process, i.e., the phase transition.

To the best of our knowledge, there are only two studies regarding the effect of phase transition on the thermal transport in SPCs. Using MD simulations, Sezginel et al.[39] studied the effect of pore expansion on the thermal conductivity of idealized MOF materials. Their study reveals that during the pore expansion process of idealized MOF crystals, the thermal conductivity increases in the direction parallel to pore expansion but remains almost unchanged in the other directions. In addition, the thermal conductivity of idealized MOF crystals is found to be strongly dependent on the tilt angle. Similarly, based on MD simulations, Lamaire et al.[40] investigated the effect of phase transition on the thermal transport in MIL-53(Al). They found that the thermal conductivity of an np phase of MIL-53(Al) is significantly larger than that of its lp phase counterpart, which is attributed to a larger vibrational density of states (VDOS) overlap between chemically bonded atom pairs after phase transition. Inspired by these studies, it is of great interest to reveal the effect of phase transition on the thermal transport property of some other important SPC series such as the isoreticular DUT crystals, which are proven to have potential applications in many specific areas.[5,11] However, the thermal transport property of these cubic SPCs after phase transition still remains unknown.

In this paper, taking the isoreticular DUT series as an example, we study the effect of phase transition on the thermal conductivity of SPCs using MD simulations together with the Green−Kubo method. Five DUT crystals including DUT-48, DUT-47, DUT-49, DUT-50, and DUT-151 are considered in our work. In contrast to most previous findings that the SPCs with larger density typically possess a larger thermal conductivity,[21,28,30,36] we demonstrate here that the np phase of a DUT-48 crystal after phase transition has a larger density but owns a smaller thermal conductivity. As for other DUT crystals including DUT-47, DUT-49, DUT-50, and DUT-151, the np phase after phase transition is found to have a higher thermal conductivity, which is as expected. This complicated effect of phase transition on the thermal transport in different SPCs is explained by the volumetric heat capacity and the VDOS analysis.

2. METHODOLOGY

2.1. Simulation Models. Atomic structures of five isoreticular DUT materials considered here, i.e., DUT-48, DUT-47, DUT-49, DUT-50, and DUT-151, are plotted in Figure 1. The ligand backbone of isoreticular DUT crystals expands from one to four units of 1,4-substituted phenylene in generating the general network architecture design for DUT-48, DUT-49, DUT-50, and DUT-151, respectively. An exception in DUT series is DUT-47 that has one unit of 2,6-substituted naphthalene, leading to an intermediate ligand length between DUT-48 and DUT-49. For the specific details of the crystal structures of these DUT materials, we refer the readers to the original synthetic report.[13] For all DUT materials considered here, we adopt a 2 × 2 × 2 supercell with periodic boundaries along three mutually perpendicular directions. As a result, DUT-48, DUT-47, DUT-49, DUT-50, and DUT-151 models considered in the present study contain 1488, 1632, 1728, 1968, and 2208 atoms, respectively. The size

https://doi.org/10.1021/acs.jpcc.1c02767
J. Phys. Chem. C 2021, 125, 12991−13001

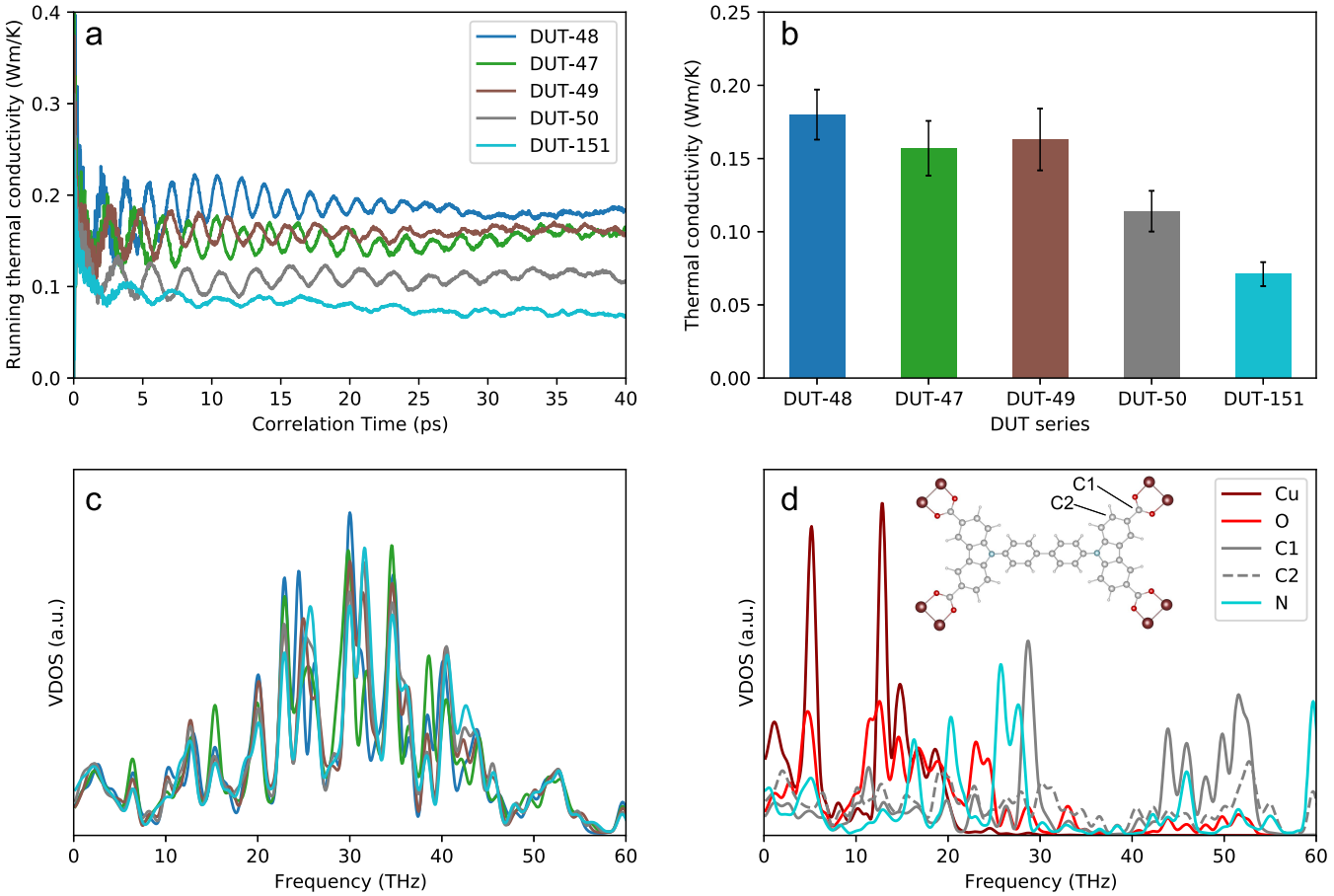

Figure 2. (a) Running thermal conductivity of isoreticular DUT crystals as a function of correlation time. (b) Calculated thermal conductivity and (c) framework VDOS distribution of isorecticular DUT crystals. Here, the thermal conductivity was calculated as the average value of 20 independent simulation raw data sets. (d) Atomic VDOS distributions of DUT-49.

selection of these DUT materials can safely exclude the size effect and, meanwhile, improve the computational efficiency because MOFs usually possess an extremely short phonon mean free path.[25]

The interactions between atoms in isoreticular DUT crystals were described by the MOF-FF force field[41] with the potential parameters extracted from the work reported by Krause et al.[13] The MOF-FF force field, which is a force field derived from first-principles calculations, has been proven to be reliable in describing the mechanical and thermal properties of SPCs, such as NGA behavior,[14,42] mechanical stability,[18] and thermal expansion of isoreticular DUT series.[43] The porosity and density of DUTs were calculated by the open-source code Zeo ++[44,45] with a probe sphere radius of 2.0 Å. The iRASPA package[46] was used for the visualization of all atomic structures.

2.2. Thermal Conductivity Calculations. The thermal conductivity of isoreticular DUT series was calculated by equilibrium MD simulations together with the Green−Kubo method.[47,48] The Green−Kubo method is based on the fluctuation−dissipation theorem,[49] which calculates the running thermal conductivity tensor k_{uv} by integrating the heat current autocorrelation function (HCACF) over a given correlation time t

$$k_{uv}(t) = \frac{V}{k_B T^2} \int_0^t \langle J_u(0) J_v(t) \rangle \mathrm{d}t \tag{1}$$

where k_B, T, and V are, respectively, Boltzmann's constant, the temperature, and the volume of the simulation box. $\langle J_u(0) J_v(t) \rangle$ is the average HCACF over different time origins with J being the heat current. Because the isoreticular DUT series investigated in this work consists of cubic crystals, their thermal properties are isotropic in three axial directions. Therefore, eq 1 can be further simplified into

$$k(t) = \frac{V}{k_B T^2} \int_0^t \langle J(0) J(t) \rangle \mathrm{d}t \tag{2}$$

All MD simulations were performed using the publicly available simulation code LAMMPS,[50] in which the velocity Verlet algorithm was used to integrate the standard Newton equations of motion. The time step was set as 0.5 fs in MD simulations. During the MD simulation process, a sufficient relaxation was performed before thermal conductivity calculations. The energy minimization was first performed using the conjugate gradient method. After that, the obtained structures were relaxed at 300 K and 0 GPa in the NPT ensemble (constant number of particles, pressure, and temperature) for 0.5 ns and, subsequently, at 300 K in the NVT ensemble (constant number of particles, volume, and temperature) for another 0.5 ns. Here, the Nose−Hoover thermostat was used to control the temperature and pressure. The thermal conductivity calculations were performed in the NVE ensemble (constant volume without thermostat). A correlation of 40 ps was adopted for all DUT crystals. The running

https://doi.org/10.1021/acs.jpcc.1c02767
J. Phys. Chem. C 2021, 125, 12991−13001

thermal conductivity would converge around 30 ps of correlation time. Thus, the thermal conductivity of all DUT crystals was obtained by averaging the values obtained at the final 10 ps. Overall, 20 independent calculations were conducted to avoid possible statistic errors and to obtain the average thermal conductivity of DUTs considered here.

2.3. Volumetric Heat Capacity and Vibrational Analysis. The volumetric heat capacity was calculated here to explain the major factor responsible for the change in the thermal conductivity of isoreticular DUT crystals. It is noted that although *PV*, i.e., the product of pressure *P* and volume *V*, fluctuates greatly in MD simulations,[51] the change of its magnitude is very small and thus can be safely ignored.[52] Under this circumstance, we directly calculated here the heat capacity $C_V(T)$ on the basis of change in the internal energy $U(T)$

$$C_V(T) \cong \frac{U(T+\Delta T) - U(T-\Delta T)}{2V\Delta T} \tag{3}$$

where T and ΔT are set as 300 and 25 K, respectively, to obtain the volumetric heat capacity of isoreticular DUT crystals at room temperature. A simulation with 2 million steps corresponding to 1 ns in the NVT ensemble was performed to achieve the gradual heating process from 275 to 325 K in MD simulations. The raw data of the obtained internal energy were averaged every 5 ps to reduce the noise. Afterward, the volumetric heat capacity can be obtained by performing a linear fitting to the obtained $U-T$ curves. To further validate the accuracy of the heat capacity obtained from the aforementioned method, we also calculated the volumetric heat capacity through energy fluctuations based on the following fluctuation−dissipation theory[53]

$$C_V(T) = \frac{\langle E^2\rangle - \langle E\rangle^2}{Vk_BT^2} \tag{4}$$

where $\langle\ \rangle$ denotes the average over simulation time. The volumetric heat capacity was obtained after 2 ns MD simulations in the NVT ensemble at room temperature 300 K. The values of volumetric heat capacity obtained from eqs 3 and 4 are compared in Table S1 (see the Supporting Information). It is found that these two methods agree very well with each other, which further proves the reliability of our calculation results from eq 3. Under this circumstance, $C_V(T)$ extracted from the directly derivative method, i.e., eq 3, was selected as the estimated volumetric heat capacity in the following discussion.

We also calculated the VDOS to further provide a microscopic insight into the lattice vibrations of DUT crystals. The VDOS was calculated by taking the following Fourier transform to the atomic velocity autocorrelation function (VACF)

$$\mathrm{VDOS}(\sigma) = \int \gamma(t) e^{-2\pi i\sigma t}\, dt \tag{5}$$

where σ is the frequency, i is the imaginary unit, $\gamma(t) = \frac{\langle \sum_i v_i(0)\cdot v_i(t)\rangle}{\langle \sum_i v_i(0)\cdot v_i(0)\rangle}$ is the VACF. Here, $v_i(t)$ and $v_0(t)$ are, respectively, velocities of ith atom at time t and the initial time. In the present study, the VACF was calculated with a simulation of over 10 ps after the structure reached its equilibrium stage. During this simulation, the velocity information after every 10 time steps was collected for calculating the VACF.

3. RESULTS AND DISCUSSION

3.1. Ligand Dependence of the Thermal Conductivity. The original lp structures of DUT crystals are first considered here. The running thermal conductivity of five DUT materials is shown in Figure 2(a) as a function of the correlation time. From this figure, we can see that although the thermal conductivity of DUTs fluctuates at the beginning of simulations, it tends to a steady value at the final 10 ps. Thus, as mentioned in Section 2.2, the averaged value at the final 10 ps was taken as the steady thermal conductivity. The obtained thermal conductivities of five DUT materials considered here are compared in Figure 2(b) and listed in Table 1. It is found that DUT-48 has the highest thermal conductivity of 0.180 W $m^{-1}K^{-1}$, followed by 0.163 W $m^{-1}K^{-1}$ of DUT-49, 0.157 W $m^{-1}K^{-1}$ of DUT-47, and 0.114 W $m^{-1}K^{-1}$ of DUT-50. DUT-151 is found to possess the lowest thermal conductivity of 0.071 W $m^{-1}K^{-1}$. Our results indicate that when compared with some other SPCs, the present isoreticular DUT crystals can be treated as thermal insulators due to the fact that they have a relatively low thermal conductivity smaller than 0.2 W $m^{-1}K^{-1}$. The low thermal conductivity observed in the present DUTs is close to the value (0.138−0.174 W $m^{-1}K^{-1}$) of their ZIF counterparts,[27,28] but is much smaller than the value of some other SPCs such as MOF-5 (0.31 W $m^{-1}K^{-1}$)[24,25] and HKUST-1 (1.65 W $m^{-1}K^{-1}$).[33,34] Moreover, it is found that the thermal conductivity of DUT crystals generally decreases with increasing ligand length. For example, when the ligand length increases from one unit of phenylene in DUT-48 to four units of phenylene in DUT-151, the thermal conductivity is found to decline from 0.180 to 0.071 W $m^{-1}K^{-1}$. A similar ligand length dependence of thermal conductivity is also observed in previous studies of IRMOF series.[21,36] The only exception is DUT-47, which possesses a ligand shorter than DUT-49 (see Figure 1) but has a thermal conductivity (0.157

Table 1. Structural Parameters and Calculated Properties of lp and np Phases of Isoreticular DUT Crytals[a]

DUT crystals	V (Å^3)	ρ (g cm^{-3})	η (%)	k (W m^{-1}K^{-1})	C_V (KJ m^{-3}K^{-1})
DUT-48(lp)	62 537	0.444	78.8	0.180	981
DUT-48(np)	25 868	0.789	55.4	0.164	1716
DUT-47(lp)	78 180	0.379	81.4	0.157	868
DUT-47(np)	41 681	0.728	59.8	0.173	1630
DUT-49(lp)	96 047	0.321	83.6	0.163	743
DUT-49(np)	46 070	0.675	62.7	0.192	1532
DUT-50(lp)	139 918	0.243	87.3	0.114	581
DUT-50(np)	58 582	0.585	66.6	0.169	1378
DUT-151(lp)	194 574	0.187	90.1	0.071	469
DUT-151(np)	75 962	0.489	71.5	0.182	1221

[a]Structural properties (volume V, density ρ, and probe-occupiable void fraction η, i.e., the porosity) were determined from the structures after energy minimization at 0 K. The thermal conductivity k and volumetric heat capacity C_V were calculated at room temperature of 300 K.

https://doi.org/10.1021/acs.jpcc.1c02767
J. Phys. Chem. C 2021, 125, 12991−13001

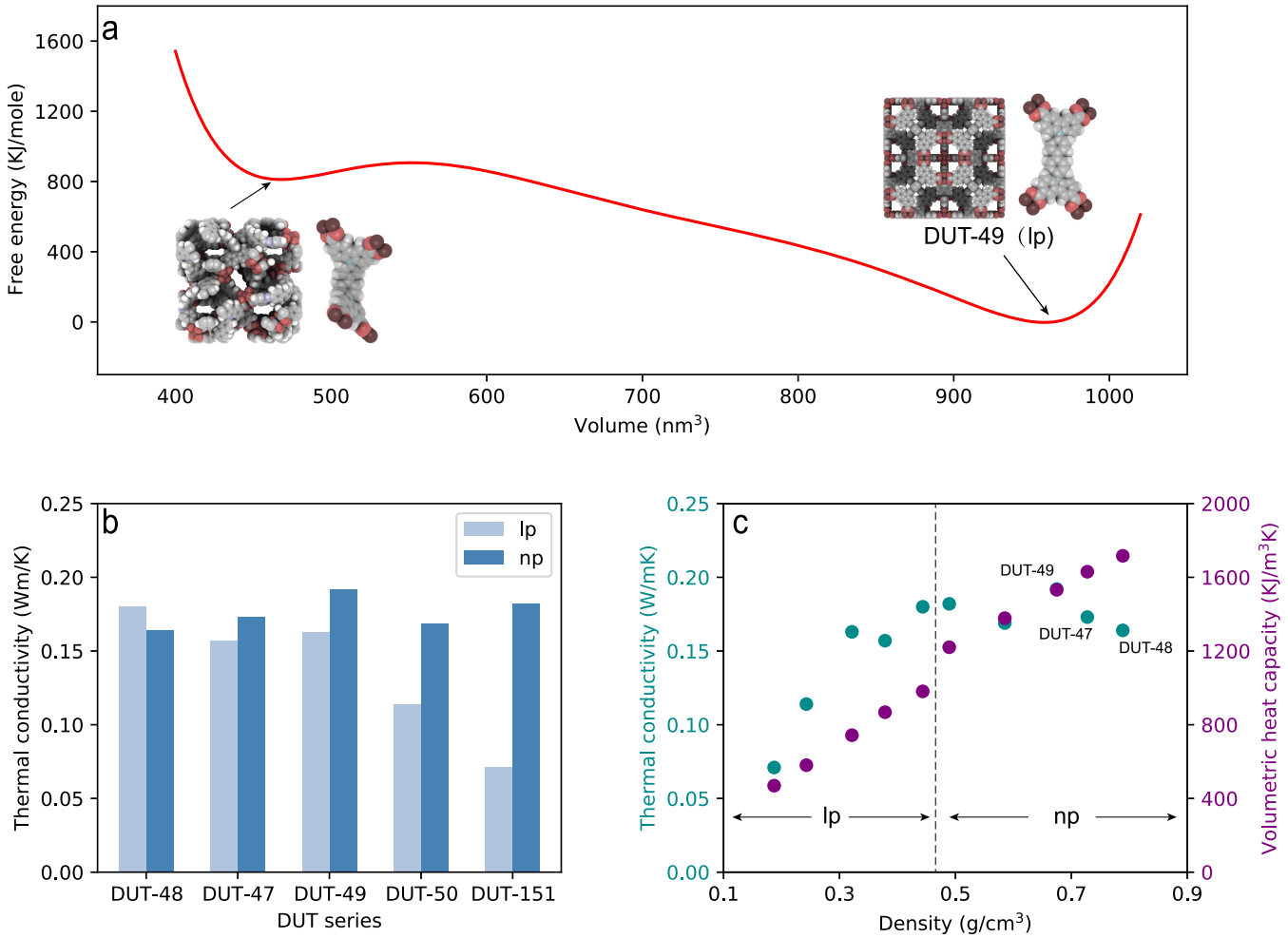

Figure 3. (a) Free energy versus volume curves of DUT-49 obtained by the *P*−*V* EOS method, and the inset shows the atomic structures of DUT-49(lp) and DUT-49(np). (b) A comparison of the thermal conductivity between lp and np phases of isoreticular DUT crystals. (c) Thermal conductivity and volumetric heat capacity of lp and np phases of isoreticular DUT crystals as a function of the density.

W m^{-1}K^{-1}) slightly lower than that of DUT-49 (0.163 W m^{-1}K^{-1}). The unique thermal transport property detected in DUT-47 materials may stem from their unique ligand backbone structure comprised by 2,6-substituted phenylene, which may cause a lattice vibrational mode slightly different from that of their counterparts with the ligand backbone constructed by 1,4-substituted phenylene. To further reveal the difference of lattice vibration among different DUTs considered here, their VDOS distributions are compared in Figure 2(c). It can be clearly observed that the VDOS of DUT-47 is different from that of other DUT crystals. For example, the VDOS peaks of DUT-47 are located around 15 THz and 38 THz, which are much higher than the values of other four DUTs. Moreover, in DUT-48, DUT-49, DUT-50, and DUT-151, the VDOS intensity is found to decrease with increasing ligand length especially around the frequency of 30 THz. This result indicates that the thermal conductivity is inversely proportional to the ligand length, which is consistent with the ligand dependence of thermal conductivity directly exacted from MD simulations of DUT materials (see Figure 2).

To explain the origin of the ultralow thermal conductivity observed in DUT crystals, we decompose the VDOS of the overall framework into each group of atoms. The VDOS distribution for the framework atoms of DUT-49 is illustrated in Figure 2(d), while results of other DUT crystals considered here are shown in Figure S1 (see the Supporting Information). The SPC can be treated as a periodic framework, in which the heat transports mainly through the bonded secondary building units.[38] Thus, the main thermal transport pathway of the isoreticular DUT materials considered here is −Cu−O−C−N−Cu− that starts from the metal atom Cu, then passes through O, C, and N atoms in the ligand backbone, and finally returns to metal atom Cu, while the function group −H is absent from this main thermal transport pathway. It is noted here that to distinguish different carbons in DUTs, the carbon atom connecting to Cu and O atoms in carboxylate moieties is termed as C1, while that in the carbon ring of a phenylene bridge (or the naphthalene bridge of DUT-47) is termed as C2. Previous studies have proven that the small overlap between the atomic VDOS of the main energy carriers of MOF materials (such as Zn and N in ZIF materials) is majorly responsible for their poor thermal transport properties..[18,23,27] As shown in Figures 2(d) and S1, the VDOS distribution of a Cu atom in all DUT crystals considered here is mainly located at a low frequency below 20 THz, while the other atoms have a broader VDOS distribution. To more directly quantify the overlap in VDOS along chemically bonded atom pairs in DUT crystals, we calculated the following similarity index $\gamma_{\alpha\text{-}\beta}$[54]

https://doi.org/10.1021/acs.jpcc.1c02767
J. Phys. Chem. C 2021, 125, 12991−13001

$$\gamma_{\alpha-\beta} = \frac{\int f_\alpha(\sigma) f_\beta(\sigma) \mathrm{d}T}{\sqrt{\int f_\alpha^2(\sigma) f_\beta^2(\sigma) \mathrm{d}T}} \quad (6)$$

which is a measure of the correlation in the chemically bonded atom pair between the spectra $f_\alpha(\sigma)$ of atom α and the spectra $f_\beta(\sigma)$ of atom β in a certain frequency range. Using this definition, in Figure S2, we graphically show the similarity index of the chemically bonded atom pairs in isoreticular DUT crystals. Because the DUT crystals share a similar framework architecture, the similarity indexes of all DUT crystals are found to be very close to each other. Specifically, as for a DUT material, the similarity index of the chemically bonded atom pair in the thermal transport path follows the order γ_{Cu-O} (0.774−0.796) > γ_{C1-C2} (0.676−0.700) and γ_{C2-N} (0.627−0.711) > γ_{O-C1} (0.470−0.493), indicating a very large overlap in the Cu−O chain, especially when compared to the O−C1 chain. From the abovementioned lattice vibrational analysis, we can see that, in addition to the effect of thermal transport resistance at the interface between the metal node and the linkers (corresponding to Cu−O chain here),[23] the large phonon mismatch of the O−C1 chain in the ligand backbone can further reduce the thermal conductivity of isoreticular DUT crystals. It should be noted that besides the different VDOS distributions existing among the present isoreticular DUT series and other MOF materials such as HKUST-1 and MOF-5, some other factors may also be responsible for the much lower thermal conductivity observed in isoreticular DUT series. For instance, according to previous studies,[36,55,56] the density and the bulk modulus are important factors determining the thermal transport property of materials. A low density and a low bulk modulus of MOF materials can result in a low thermal conductivity in them. From Table 1, the isoreticular DUT series is found to have a density in the range of 0.187−0.444 g cm^{-3}, which is much lower than 0.555 g cm^{-3} of MOF-5 and 0.851 g cm^{-3} of HKUST-1.[21] Meanwhile, as illustrated in Table S2 in the Supporting Information, the isoreticular DUT series possesses a bulk modulus in the range of 4.0−12.0 GPa, which is smaller than 13.6 GPa of MOF-5 and 23.9 GPa of HKUST-1.[55] Thus, it is reasonable to deduce that the lower density and smaller bulk modulus of DUT series are other possible factors inducing the weaker thermal transport property in DUT materials when compared to their HKUST-1 and MOF-5 counterparts. According to the classical phonon−gas model, the thermal conductivity of a crystal can be written as[57,58]

$$k = \frac{1}{3} C_V v_g l_{eff} \quad (7)$$

where C_V is the volumetric heat capacity, v_g is the group velocity of a phonon, and l_{eff} is the mean free path of phonon. This model suggests that the thermal conductivity of a crystal is proportional to its volumetric heat capacity, phonon group velocity, and the phonon mean free path. Table 1 shows the structural parameters (lattice volume, density, and porosity) and the calculated thermal properties (thermal conductivity and volumetric heat capacity) of lp and np phases of DUT crystals. It is found that the thermal conductivity of DUT crystals within the lp phase generally increases with growing volumetric heat capacity, as shown in Figure S3. Because the volumetric heat capacity of DUT crystals is proportional to the density and is inversely proportional to the porosity, as plotted in Figure S4, the decreased volumetric heat capacity of the DUT series ranging from DUT-48 to DUT-151 is thus responsible for the evolution of thermal conductivity of isoreticular DUT crystals with different ligands, as shown in Figure 2(b). Moreover, the thermal conductivity of isoreticular DUT crystals with different densities or porosities graphically shown in Figures 3(b) and S5 is found to decrease with decreasing density or with increasing pore size. The same dependence of thermal conductivity on the density or porosity is also observed in previous studies of the idealized MOFs.[36]

3.2. Influence of Phase Transition on the Thermal Conductivity. The pressure versus volume equations of state ($P-V$ EOS) method was applied to obtain the np phase of DUT crystals. This method has been widely used in previous studies in investigating the mechanical instability and dynamic effects of SPCs.[13,16,18,42,59−64] The theories and simulation details of the $P-V$ EOS method are provided in the Supporting Information. Taking DUT-49 as an example, Figure 3(a) shows the free-energy evolution with shrinking volume. Two extreme points correspond to the lp and np phases of DUT-49, i.e., DUT-49(lp) and DUT-49(np), respectively. As shown in the atomic structures presented in Figure 3(a), the phase transition of DUT series is driven by the buckling of their ligands.[18] The calculated thermal conductivity of the transformed np structures of various DUT materials is shown in Figure 3(b), in which the result of their parent lp counterparts is shown as well. Meanwhile, the corresponding specific values of the obtained thermal conductivity are also listed in Table 1. It is found that expect DUT-48 whose np phase has a thermal conductivity (0.164 W m^{-1}K^{-1}) smaller than that of its lp phase (0.180 W m^{-1}K^{-1}), the thermal conductivity of the transformed np phase of all other DUT materials is higher than that of their parent lp phase. Especially, as for DUT-50 and DUT-151, the thermal conductivity of their np phase after the phase transition can be, respectively, 48 and 156% larger than the value of their parent lp phase. Moreover, among all DUT crystals considered here, the np structure of DUT-49, i.e., DUT-49(np), shows the highest thermal conductivity of 0.192 W m^{-1}K^{-1}. In Figure 3(c), we graphically show the thermal conductivity (k) and the volumetric heat capacity (C_V) as a function of the density (ρ) of both phases of different isoreticular DUT crystals considered here. From this figure, we find that C_V increases linearly with growing ρ in both lp and np phases of DUTs. However, as for lp and np phases of DUTs, their k exhibits different relations with ρ. It is found that k of the lp phase increases generally with growing ρ, while k of the np phase seems to be independent of ρ, which fluctuates around 0.16 W m^{-1}K^{-1}. According to the classical phonon−gas model shown in eq 7, the thermal conductivity of a material is expected to increase with growing density or heat capacity. Actually, this conventional relation between thermal conductivity and density has been observed in many previous studies on typical SPCs.[21,36] However, in DUT materials after phase transition, especially in DUT-49(np), DUT-47(np), and DUT-48(np), k is oppositely found to decrease with growing ρ or C_V. Actually, the conventional relation between thermal conductivity and density is similarly found to be broken in the SPCs with a tilted bond orientation because now the impact of the bond orientation on thermal conductivity of idealized SPCs is found to be more important than that of the density change.[39] These results indicate that the thermal conductivity of SPCs under some specific conditions such as enduring phase transition studied here and possessing titled bond orientation considered previously[39] is not dominated by the volumetric

https://doi.org/10.1021/acs.jpcc.1c02767
J. Phys. Chem. C 2021, 125, 12991−13001

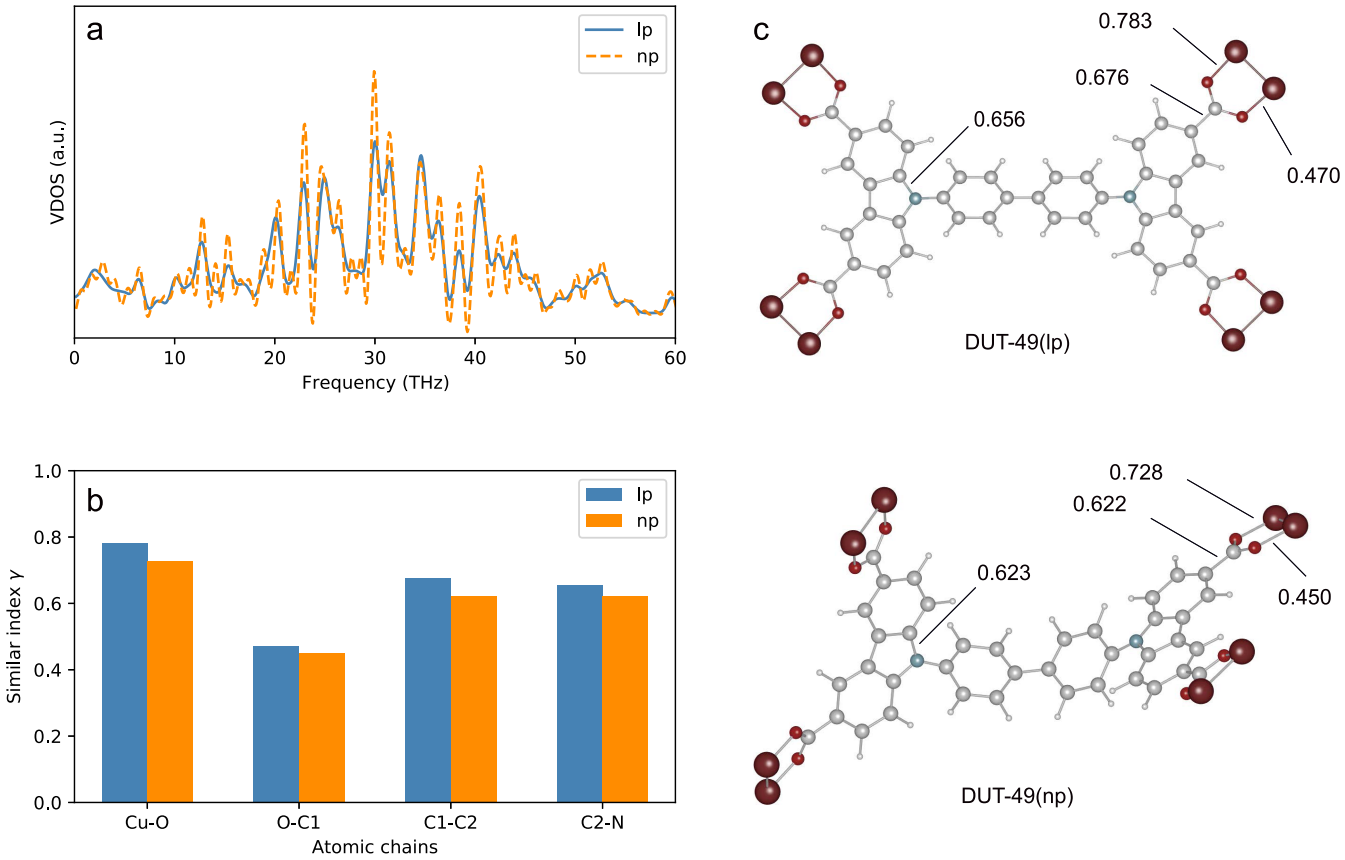

Figure 4. (a) Framework VDOS of lp and np phases of DUT-49. (b) Similarity index γ of the chains in lp and np phases of DUT-49. (c) Similarity index γ in the chemically bonded atom pairs of lp and np phases of DUT-49.

heat capacity. The phonon properties such as the phonon group velocity and the phonon mean free path now may have a crucial effect on the thermal transport in SPC crystals, which will be discussed in detail later.

To investigate the different thermal transport properties observed in lp and np structures of DUTs, we compare the VDOS distribution of the lp and np phases of DUT-49 in Figure 4(a). The results of other DUT crystals considered here are shown in Figure S6. As for all DUT crystals, more modes and peaks are observed in the VDOS distribution of their np phase. To further evaluate the change in the VDOS overlap caused by the phase transition, we compare the similarity index of lp and np phases of DUT-49 in Figure 4(b,c). A similar comparison of other DUT crystals is shown in Figure S7. In general, the similarity index of chemically bonded atom pairs in the lp phase of all DUT crystals is larger than that in the np phase, which corresponds to a decrease of the VDOS overlap after phase transition. This result indicates that compared to their lp counterparts, the np structures of DUT crystals possess a higher thermal resistance and more significant phonon scattering between the chemically bonded atom pairs, which would thus weaken the thermal transport properties. Very recently, Lamiare et al.[40] demonstrated that the VDOS overlap between the chemically bonded atom pairs in the np phase of MIL-53(Al) is much larger than that of its lp counterpart, which is in contrast to the case of isoreticular DUT crystals discussed here. This difference observed between these two MOF materials might originate from their different mechanisms of phase transition. The phase transition of DUT crystals is accompanied by the buckling of their ligand backbones,[13,14,28] as shown in Figure 3(b), while the ligand backbones of MIL-53(Al) remain straight at both lp and np phases. Because the phonon scattering in the buckled ligand is more significant than that in the pristine straight ligand,[65] DUT crystals after phase transition are thus expected to possess a lower thermal conductivity.

It is known that materials with a low elastic modulus usually have flattened phonon dispersion curves, which correspond to low phonon group velocities in these materials. According to eq 6, the thermal conductivity is directly proportional to the phonon group velocity. Thus, materials with a lower elastic modulus are expected to possess a lower thermal conductivity.[56,66,67] Here, we adopt the stress-fluctuation method[68] to calculate the elastic constants and mechanical properties of lp and np phases of five isoreticular DUT crystals. The theory of the stress-fluctuation method and simulation detail for calculating the mechanical properties are both presented in the Supporting Information. Due to the very high symmetry of their lattice structures, the cubic isoreticular DUT crystals only have three independent elastic constants, which are C_{11}, C_{12}, and C_{44}, as listed in Table S2. The corresponding mechanical properties including Young's modulus, shear modulus, and bulk modulus of np and np phases of different isoreticular DUT crystals considered here are compared in Figure 5. As for DUT materials within the lp phase, their Young's modulus, shear modulus, and bulk modulus are found to decrease from 21.0, 8.7, and 12.0 GPa of DUT-48 with a porosity of 78.8% to 4.7, 1.8, and 4.0 GPa of DUT-151 with a porosity of 90.1%. As shown in Figures 5(a–c), the elastic moduli of the np phase of all DUT crystals are

https://doi.org/10.1021/acs.jpcc.1c02767
J. Phys. Chem. C 2021, 125, 12991−13001

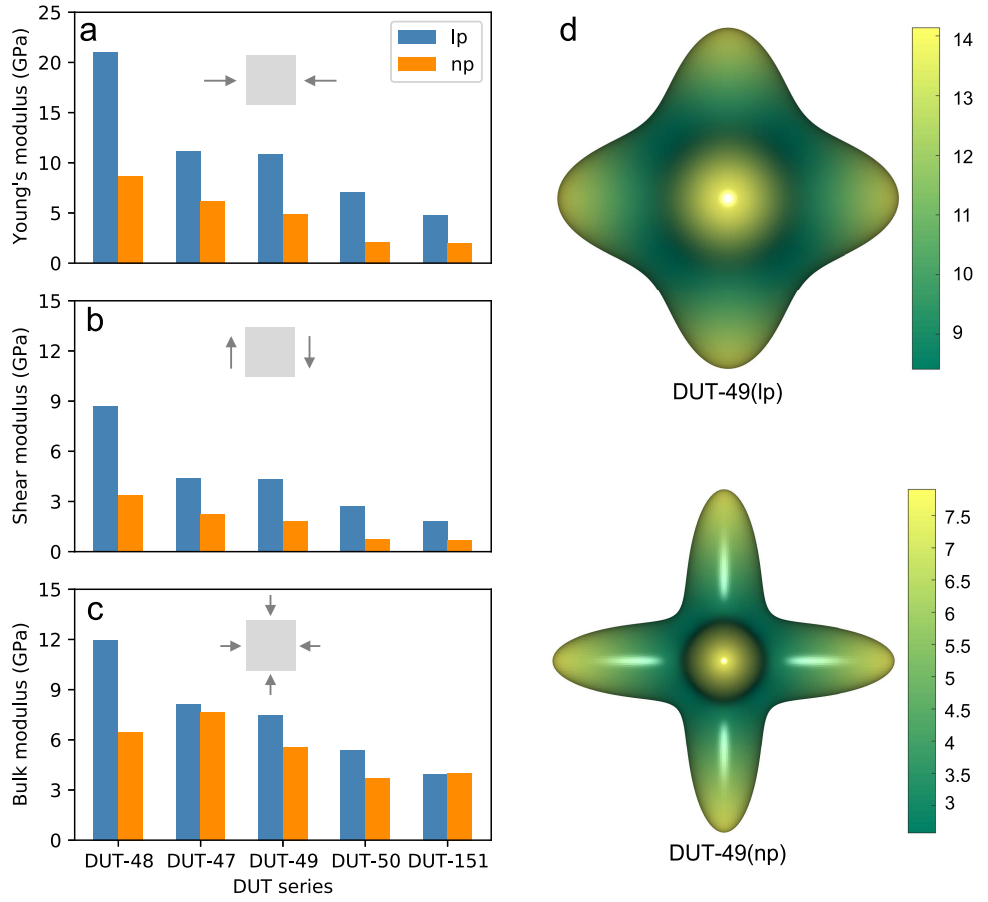

Figure 5. Mechanical properties including (a) Young's modulus, (b) shear modulus, and (c)bulk modulus of lp and np phases of isoreticular DUT crystals. The inset shows the deformation mode corresponding to each modulus. (d) Spatial dependence of Young's modulus of lp and np phases of DUT-49. All results are in the unit of GPa.

generally found to be smaller than those of their lp counterpart. The only exception is the bulk modulus of DUT-151, whose np phase possesses a value slightly larger than that of its lp phase. The weaker mechanical properties generally observed in the np phase of DUTs can be attributed to the predistorted structure of the buckled ligand backbone of DUT materials, which exhibits the higher compressibility when compared to the straight ligand backbone of the parent lp phase.[28,69] We also plot the spatial dependence of Young's modulus of DUT-49 in Figure 5(d). The corresponding results of other DUT materials are shown in Figure S8. From Figures 5(d) and S8, we can see that the softening of Young's modulus induced by the phase transition is independent of the crystal direction. From the abovementioned results, we can see that the reduction of elastic moduli of DUTs from a lp phase to an np phase will reduce the phonon velocity, which will result in a lower thermal conductivity of isoreticular DUT crystals after phase transition.

From the above discussion, we can see that the phase transition of DUT crystals from the parent lp phase to the transformed np phase can affect the thermal transport by changing the volumetric heat capacity and also the phonon properties including phonon scattering intensity and phonon group velocity. On the one hand, the volume shrinkage induced by the phase transition will result in a great increase of the volumetric heat capacity, which can enhance the thermal conductivity of DUTs. On the other hand, the ligand buckling accompanied with the phase transition can aggravate the phonon scattering and cause a reduction in the phonon group velocity, which will weaken the thermal transport property of DUTs. The mechanism of the competition between above two effects on the thermal conductivity of DUTs after phase transition is schematically shown in Figure 6. Because the thermal conductivity of DUT-48 is reduced after phase transition (see Figure 3), the increased phonon scattering plays the dominant role. However, in other DUTs, including DUT-47, DUT-49, DUT-50, and DUT-151, the effect of volumetric heat capacity becomes dominant, which results in a higher thermal conductivity in their transformed np phase. To clearly measure the influence of phase transition on the thermal conductivity of DUT materials considered here, we introduce an evaluation parameter α defined as $\alpha = (k_{np} - k_{lp})/k_{lp}$, where k_{lp} and k_{np} are values of the thermal conductivity of lp and np phases of DUT materials, respectively. Thus, $\alpha > 0$ indicates that the phase transition enhances the thermal transport properties, while $\alpha < 0$ indicates the opposite effect of the phase transition. We graphically show α of DUT materials with different porosities in Figure 6. It is found that the value of α increases with growing porosity. Moreover, the largest enhancement in the thermal conductivity is found in DUT-151 after phase transition, which can be attributed to the fact that its ultraporous DUT crystal can result in a great increase of its volumetric heat capacity after phase transition.

https://doi.org/10.1021/acs.jpcc.1c02767
J. Phys. Chem. C 2021, 125, 12991−13001

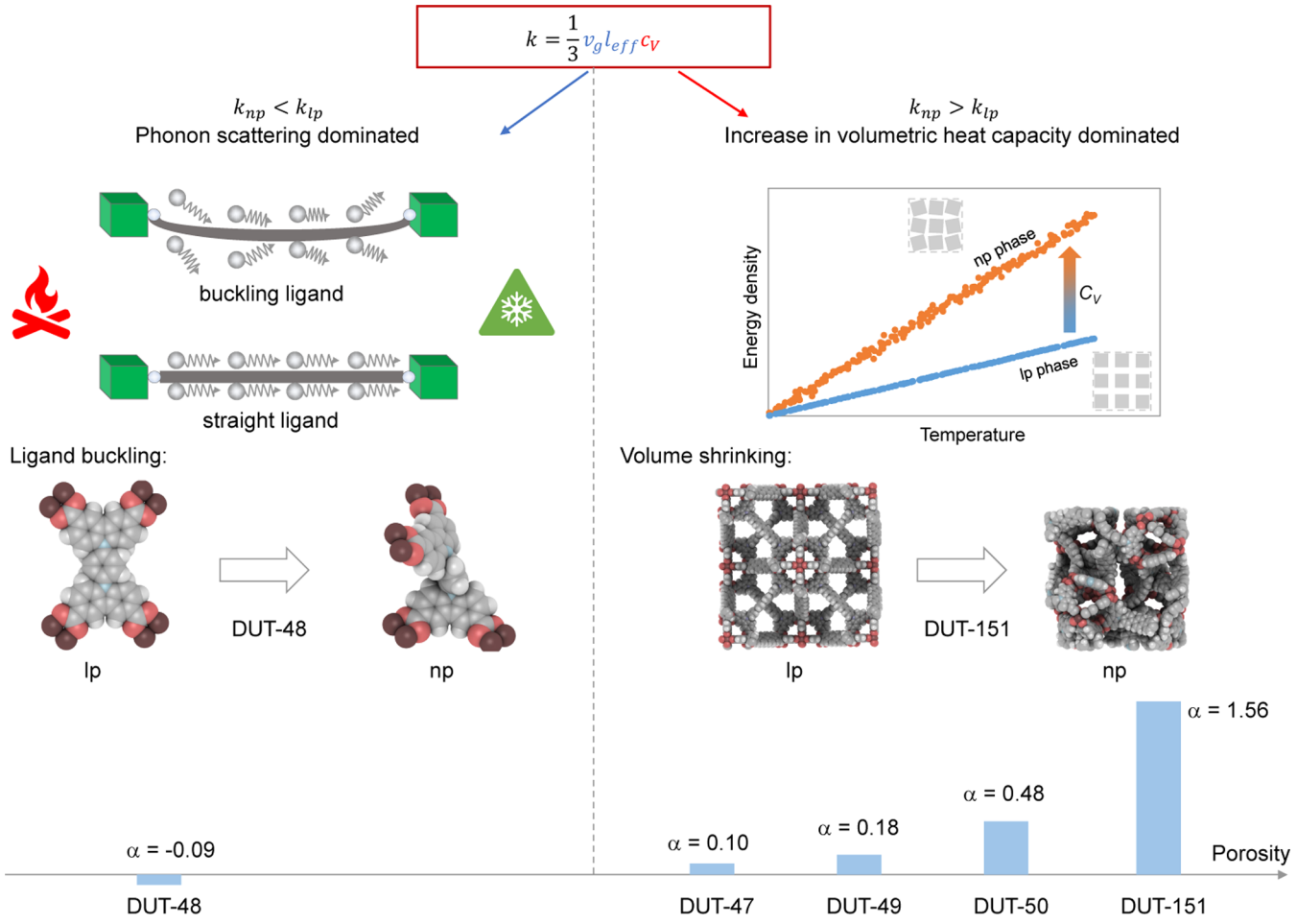

Figure 6. (Top) Schematics illustrating the competitive mechanism between enhanced phonon scattering and increased volumetric heat capacity after phase transition of isoreticular DUT materials. (Bottom) Evaluation parameter α of five DUT materials as a function of their porosity.

4. CONCLUSIONS

Taking the isoreticular DUT materials, including DUT-48, DUT-47, DUT-49, DUT-50, and DUT-151, as an example, in this paper, we comprehensively investigate the effect of phase transition on the thermal transport in SPCs using MD simulations together with the Green−Kubo method. It is shown that the pristine DUT materials have a very low thermal conductivity smaller than 0.2 W $m^{-1}K^{-1}$. The ultralow thermal conductivity observed in DUTs can be attributed to the thermal transport resistance in the O−C chain observed in the present VDOS analysis as well as the interface between the metal node and the organic linker reported previously. Regarding the influence of phase transition, the thermal conductivity of the transformed np phase of DUT-48 is slightly smaller than that of its parent lp phase. However, as for other DUT materials, i.e., DUT-47, DUT-49, DUT-50, and DUT-151, the np phase exhibits a higher thermal conductivity. Especially, the thermal conductivity of the np phase of DUT-151 can be up to 155.8% larger than that of its lp phase. This complicated effect of phase transition on the thermal conductivity of isoreticular DUT materials is explained by the mechanism of the competition between the enhanced phonon scattering and the increased volumetric heat capacity after phase transition. As for the DUT-48 having a relatively small porosity, the enhanced phonon scattering plays the dominant role, which leads to a lower thermal conductivity of its np phase. However, the increased volumetric heat capacity becomes the dominant effect in other DUT materials with a relatively large porosity, which results in the increase of thermal conductivity after phase transition. Overall, we find that although the density of some SPCs can be greatly increased after phase transition, their thermal conductivity can be significantly reduced in this process. This finding can greatly expand current knowledge about the thermal conductivity of MOFs that was previously found to grow usually with increasing density.

■ ASSOCIATED CONTENT

Supporting Information

The Supporting Information is available free of charge at https://pubs.acs.org/doi/10.1021/acs.jpcc.1c02767.

VDOS distribution for the framework atoms of DUT crystals, the similarity index between chemically bonded atom pairs in DUT crystals, the volumetric heat capacity-dependent and porosity-dependent thermal conductivity of the lp phase of DUT crystals, the volumetric heat capacity of DUT crystals with different densities and porosities, comparison of the framework VDOS, the similarity index γ between chemically bonded atom pairs, and spatial dependence of Young's modulus of lp and np phases of DUT crystals (PDF)

https://doi.org/10.1021/acs.jpcc.1c02767
J. Phys. Chem. C 2021, 125, 12991−13001

AUTHOR INFORMATION

Corresponding Authors

Jin Zhang − *School of Science, Harbin Institute of Technology, Shenzhen 518055, P. R. China*; Email: jinzhang@hit.edu.cn

Zheng Zhong − *School of Science, Harbin Institute of Technology, Shenzhen 518055, P. R. China*; orcid.org/0000-0001-5293-7098; Email: zhongzheng@hit.edu.cn

Author

Penghua Ying − *School of Science, Harbin Institute of Technology, Shenzhen 518055, P. R. China*

Complete contact information is available at: https://pubs.acs.org/10.1021/acs.jpcc.1c02767

Notes

The authors declare no competing financial interest.

ACKNOWLEDGMENTS

This study was supported by the National Key R&D Program of China (no. 2018YFB1502602) and the National Natural Science Foundation of China (nos. 11932005 and 11772106).

REFERENCES

(1) Horike, S.; Shimomura, S.; Kitagawa, S. Soft porous crystals. *Nat. Chem.* **2009**, *1*, 695.

(2) Schneemann, A.; Bon, V.; Schwedler, I.; Senkovska, I.; Kaskel, S.; Fischer, R. A. Flexible metal-organic frameworks. *Chem. Soc. Rev.* **2014**, *43*, 6062−6096.

(3) Evans, J. D.; Bon, V.; Senkovska, I.; Lee, H.-C.; Kaskel, S. Four-dimensional metal-organic frameworks. *Nat. Commun.* **2020**, *11*, No. 2690.

(4) Coudert, F.-X. Responsive metal-organic frameworks and framework materials: under pressure, taking the heat, in the spotlight, with friends. *Chem. Mater.* **2015**, *27*, 1905−1916.

(5) Krause, S.; Hosono, N.; Kitagawa, S. Chemistry of Soft Porous Crystals-Structural Dynamics and Gas Adsorption Properties. *Angew. Chem., Int. Ed.* **2020**, *52*, 15325−15341.

(6) Ghoufi, A.; Benhamed, K.; Boukli-Hacene, L.; Maurin, G. Electrically induced breathing of the MIL-53 (Cr) metal-organic framework. *ACS Cent. Sci.* **2017**, *3*, 394−398.

(7) Coudert, F.-X.; Evans, J. D. Nanoscale metamaterials: meta-MOFs and framework materials with anomalous behavior. *Coord. Chem. Rev.* **2019**, *388*, 48−62.

(8) Mason, J. A.; Oktawiec, J.; Taylor, M. K.; Hudson, M. R.; Rodriguez, J.; Bachman, J. E.; Gonzalez, M. I.; Cervellino, A.; Guagliardi, A.; Brown, C. M.; et al. Methane storage in flexible metal-organic frameworks with intrinsic thermal management. *Nature* **2015**, *527*, 357−361.

(9) Sato, H.; Kosaka, W.; Matsuda, R.; Hori, A.; Hijikata, Y.; Belosludov, R. V.; Sakaki, S.; Takata, M.; Kitagawa, S. Self-accelerating CO sorption in a soft nanoporous crystal. *Science* **2014**, *343*, 167−170.

(10) Van Assche, T. R.; Baron, G. V.; Denayer, J. F. Molecular separations with breathing metal-organic frameworks: modelling packed bed adsorbers. *Dalton Trans.* **2016**, *45*, 4416−4430.

(11) Krause, S.; Bon, V.; Senkovska, I.; Stoeck, U.; Wallacher, D.; Többens, D. M.; Zander, S.; Pillai, R. S.; Maurin, G.; Coudert, F.-X.; et al. A pressure-amplifying framework material with negative gas adsorption transitions. *Nature* **2016**, *532*, 348−352.

(12) Yaghi, O. M.; O'Keeffe, M.; Ockwig, N. W.; Chae, H. K.; Eddaoudi, M.; Kim, J. Reticular synthesis and the design of new materials. *Nature* **2003**, *423*, 705−714.

(13) Krause, S.; Evans, J. D.; Bon, V.; Senkovska, I.; Iacomi, P.; Kolbe, F.; Ehrling, S.; Troschke, E.; Getzschmann, J.; Többens, D. M.; et al. Towards general network architecture design criteria for negative gas adsorption transitions in ultraporous frameworks. *Nat. Commun.* **2019**, *10*, No. 3632.

(14) Krause, S.; Evans, J. D.; Bon, V.; Senkovska, I.; Ehrling, S.; Iacomi, P.; Többens, D. M.; Wallacher, D.; Weiss, M. S.; Zheng, B.; et al. Engineering micromechanics of soft porous crystals for negative gas adsorption. *Chem. Sci.* **2020**, *11*, 9468−9479.

(15) Evans, J. D.; Krause, S.; Kaskel, S.; Sweatman, M. B.; Sarkisov, L. Exploring the thermodynamic criteria for responsive adsorption processes. *Chem. Sci.* **2019**, *10*, 5011−5017.

(16) Vanduyfhuys, L.; Rogge, S.; Wieme, J.; Vandenbrande, S.; Maurin, G.; Waroquier, M.; Van Speybroeck, V. Thermodynamic insight into stimuli-responsive behaviour of soft porous crystals. *Nat. Commun.* **2018**, *9*, No. 204.

(17) Vanduyfhuys, L.; Van Speybroeck, V. Unraveling the thermodynamic conditions for negative gas adsorption in soft porous crystals. *Commun. Phys.* **2019**, *2*, No. 102.

(18) Ying, P.; Zhang, J.; Zhong, Z. Pressure-induced phase transition of isoreticular MOFs: Mechanical instability due to ligand buckling. *Microporous Mesoporous Mater.* **2020**, *312*, No. 110765.

(19) Erickson, K. J.; Léonard, F.; Stavila, V.; Foster, M. E.; Spataru, C. D.; Jones, R. E.; Foley, B. M.; Hopkins, P. E.; Allendorf, M. D.; Talin, A. A. Thin film thermoelectric metal-organic framework with high Seebeck coefficient and low thermal conductivity. *Adv. Mater.* **2015**, *27*, 3453−3459.

(20) Gunatilleke, W. D.; Wei, K.; Niu, Z.; Wojtas, L.; Nolas, G.; Ma, S. Thermal conductivity of a perovskite-type metal-organic framework crystal. *Dalton Trans.* **2017**, *46*, 13342−13344.

(21) Wieme, J.; Vandenbrande, S.; Lamaire, A.; Kapil, V.; Vanduyfhuys, L.; Van Speybroeck, V. Thermal Engineering of Metal-Organic Frameworks for Adsorption Applications: A Molecular Simulation Perspective. *ACS Appl. Mater. Interfaces* **2019**, *11*, 38697−38707.

(22) Maurin, G.; Serre, C.; Cooper, A.; Férey, G. The new age of MOFs and of their porous-related solids. *Chem. Soc. Rev.* **2017**, *46*, 3104−3107.

(23) Wieser, S.; Kamencek, T.; Dürholt, J. P.; Schmid, R.; Bedoya-Martínez, N.; Zojer, E. Identifying the Bottleneck for Heat Transport in Metal-Organic Frameworks. *Adv. Theory Simul.* **2020**, *4*, No. 2000211.

(24) Han, L.; Budge, M.; Greaney, P. A. Relationship between thermal conductivity and framework architecture in MOF-5. *Comput. Mater. Sci.* **2014**, *94*, 292−297.

(25) Huang, B.; McGaughey, A.; Kaviany, M. Thermal conductivity of metal-organic framework 5 (MOF-5): Part I. Molecular dynamics simulations. *Int. J. Heat Mass Transfer* **2007**, *50*, 393−404.

(26) Huang, B.; Ni, Z.; Millward, A.; McGaughey, A.; Uher, C.; Kaviany, M.; Yaghi, O. Thermal conductivity of a metal-organic framework (MOF-5): Part II. Measurement. *Int. J. Heat Mass Transfer* **2007**, *50*, 405−411.

(27) Zhang, X.; Jiang, J. Thermal conductivity of zeolitic imidazolate framework-8: A molecular simulation study. *J. Phys. Chem. C* **2013**, *117*, 18441−18447.

(28) Ying, P.; Zhang, J.; Zhang, X.; Zhong, Z. Impacts of Functional Group Substitution and Pressure on the Thermal Conductivity of ZIF-8. *J. Phys. Chem. C* **2020**, *124*, 6274−6283.

(29) Wei, W.; Huang, J.; Li, W.; Peng, H.; Li, S. Impacts of Ethanol and Water Adsorptions on Thermal Conductivity of ZIF-8. *J. Phys. Chem. C* **2019**, *123*, 27369−27374.

(30) Sørensen, S. S.; Østergaard, M. B.; Stepniewska, M.; Johra, H.; Yue, Y.; Smedskjaer, M. M. Metal-Organic Framework Glasses Possess Higher Thermal Conductivity than Their Crystalline Counterparts. *ACS Appl. Mater. Interfaces* **2020**, *12*, 18893−18903.

(31) Huang, J.; Fan, A.; Xia, X.; Li, S.; Zhang, X. In Situ Thermal Conductivity Measurement of Single-Crystal Zeolitic Imidazolate Framework-8 by Raman-Resistance Temperature Detectors Method. *ACS Nano* **2020**, *14*, 14100−14107.

(32) Cui, B.; Audu, C. O.; Liao, Y.; Nguyen, S. T.; Farha, O. K.; Hupp, J. T.; Grayson, M. Thermal conductivity of zif-8 thin-film

under ambient gas pressure. *ACS Appl. Mater. Interfaces* **2017**, *9*, 28139−28143.
(33) Islamov, M.; Babaei, H.; Wilmer, C. E. Influence of Missing Linker Defects on the Thermal Conductivity of Metal-Organic Framework HKUST-1. *ACS Appl. Mater. Interfaces* **2020**, *12*, 56172−56177.
(34) Babaei, H.; DeCoster, M. E.; Jeong, M.; Hassan, Z. M.; Islamoglu, T.; Baumgart, H.; McGaughey, A. J.; Redel, E.; Farha, O. K.; Hopkins, P. E.; et al. Observation of reduced thermal conductivity in a metal-organic framework due to the presence of adsorbates. *Nat. Commun.* **2020**, *11*, No. 4010.
(35) Babaei, H.; Wilmer, C. E. Mechanisms of heat transfer in porous crystals containing adsorbed gases: Applications to metal-organic frameworks. *Phys. Rev. Lett.* **2016**, *116*, No. 025902.
(36) Babaei, H.; McGaughey, A. J.; Wilmer, C. E. Effect of pore size and shape on the thermal conductivity of metal-organic frameworks. *Chem. Sci.* **2017**, *8*, 583−589.
(37) Sezginel, K. B.; Asinger, P. A.; Babaei, H.; Wilmer, C. E. Thermal transport in interpenetrated metal-organic frameworks. *Chem. Mater.* **2018**, *30*, 2281−2286.
(38) Cheng, R.; Li, W.; Wei, W.; Huang, J.; Li, S. Molecular Insights into the Correlation between Microstructure and Thermal Conductivity of Zeolitic Imidazolate Frameworks. *ACS Appl. Mater. Interfaces* **2021**, *13*, 14141−14149.
(39) Sezginel, K. B.; Lee, S.; Babaei, H.; Wilmer, C. E. Effect of Flexibility on Thermal Transport in Breathing Porous Crystals. *J. Phys. Chem. C* **2020**, *124*, 18604−18608.
(40) Lamaire, A.; Wieme, J.; Hoffman, A. E.; Van Speybroeck, V. Atomistic insight in the flexibility and heat transport properties of the stimuli-responsive metal-organic framework MIL-53 (Al) for water-adsorption applications using molecular simulations. *Faraday Discuss.* **2020**, *225*, 301−323.
(41) Bureekaew, S.; Amirjalayer, S.; Tafipolsky, M.; Spickermann, C.; Roy, T. K.; Schmid, R. MOF-FF-A flexible first-principles derived force field for metal-organic frameworks. *Phys. Status Solidi (b)* **2013**, *250*, 1128−1141.
(42) Evans, J. D.; Bocquet, L.; Coudert, F.-X. Origins of negative gas adsorption. *Chem* **2016**, *1*, 873−886.
(43) Evans, J. D.; Dürholt, J. P.; Kaskel, S.; Schmid, R. Assessing negative thermal expansion in mesoporous metal-organic frameworks by molecular simulation. *J. Mater. Chem. A* **2019**, *7*, 24019−24026.
(44) Willems, T. F.; Rycroft, C. H.; Kazi, M.; Meza, J. C.; Haranczyk, M. Algorithms and tools for high-throughput geometry-based analysis of crystalline porous materials. *Microporous Mesoporous Mater.* **2012**, *149*, 134−141.
(45) Ongari, D.; Boyd, P. G.; Barthel, S.; Witman, M.; Haranczyk, M.; Smit, B. Accurate characterization of the pore volume in microporous crystalline materials. *Langmuir* **2017**, *33*, 14529−14538.
(46) Dubbeldam, D.; Calero, S.; Vlugt, T. J. iRASPA: GPU-accelerated visualization software for materials scientists. *Mol. Simul.* **2018**, *44*, 653−676.
(47) Green, M. S. Markoff random processes and the statistical mechanics of time-dependent phenomena. II. Irreversible processes in fluids. *J. Chem. Phys.* **1954**, *22*, 398−413.
(48) Kubo, R. Statistical-mechanical theory of irreversible processes. I. General theory and simple applications to magnetic and conduction problems. *J. Phys. Soc. Jpn.* **1957**, *12*, 570−586.
(49) Haile, J.; Johnston, I.; Mallinckrodt, A. J.; McKay, S. Molecular dynamics simulation: elementary methods. *Comput. Phys.* **1993**, *7*, 625.
(50) Plimpton, S. Fast parallel algorithms for short-range molecular dynamics. *J. Comput. Phys.* **1995**, *117*, 1−19.
(51) Gaillac, R.; Pullumbi, P.; Beyer, K. A.; Chapman, K. W.; Keen, D. A.; Bennett, T. D.; Coudert, F.-X. Liquid metal-organic frameworks. *Nat. Mater.* **2017**, *16*, 1149−1154.
(52) Yang, Y.; Shin, Y. K.; Li, S.; Bennett, T. D.; van Duin, A. C.; Mauro, J. C. Enabling computational design of ZIFs using ReaxFF. *J. Phys. Chem. B* **2018**, *122*, 9616−9624.
(53) Marconi, U. M. B.; Puglisi, A.; Rondoni, L.; Vulpiani, A. Fluctuation-dissipation: response theory in statistical physics. *Phys. Rep.* **2008**, *461*, 111−195.
(54) Hoffman, A. E.; Vanduyfhuys, L.; Nevjestic, I.; Wieme, J.; Rogge, S. M.; Depauw, H.; Van Der Voort, P.; Vrielinck, H.; Van Speybroeck, V. Elucidating the vibrational fingerprint of the flexible metal-organic framework MIL-53 (Al) using a combined experimental/computational approach. *J. Phys. Chem. C* **2018**, *122*, 2734−2746.
(55) Boyd, P. G.; Moosavi, S. M.; Witman, M.; Smit, B. Force-field prediction of materials properties in metal-organic frameworks. *J. Phys. Chem. Lett.* **2017**, *8*, 357−363.
(56) Kim, W. Strategies for engineering phonon transport in thermoelectrics. *J. Mater. Chem. C* **2015**, *3*, 10336−10348.
(57) Kittel, C.; McEuen, P.; McEuen, P. *Introduction to Solid State Physics*; Wiley: New York, 1996; Vol. *8*.
(58) Zhang, Z. M.; Zhang, Z. M.; Luby *Nano/microscale Heat Transfer*; Springer, 2007.
(59) Rogge, S. M.; Waroquier, M.; Van Speybroeck, V. Unraveling the thermodynamic criteria for size-dependent spontaneous phase separation in soft porous crystals. *Nat. Commun.* **2019**, *10*, No. 4842.
(60) Wieme, J.; Lejaeghere, K.; Kresse, G.; Van Speybroeck, V. Tuning the balance between dispersion and entropy to design temperature-responsive flexible metal-organic frameworks. *Nat. Commun.* **2018**, *9*, No. 4899.
(61) Demuynck, R.; Rogge, S. M.; Vanduyfhuys, L.; Wieme, J.; Waroquier, M.; Van Speybroeck, V. Efficient construction of free energy profiles of breathing metal-organic frameworks using advanced molecular dynamics simulations. *J. Chem. Theory Comput.* **2017**, *13*, 5861−5873.
(62) Keupp, J.; Schmid, R. Molecular dynamics simulations of the "breathing" phase transformation of MOF nanocrystallites. *Adv. Theory Simul.* **2019**, *2*, No. 1900117.
(63) Vervoorts, P.; Keupp, J.; Schneemann, A.; Hobday, C. L.; Daisenberger, D.; Fischer, R. A.; Schmid, R.; Kieslich, G. Configurational Entropy Driven High-Pressure Behaviour of a Flexible Metal-Organic Framework (MOF). *Angew. Chem.* **2020**, *133*, No. 1047.
(64) Rogge, S. M.; Waroquier, M.; Van Speybroeck, V. Reliably modeling the mechanical stability of rigid and flexible metal-organic frameworks. *Acc. Chem. Res.* **2018**, *51*, 138−148.
(65) Zhang, J. Phase transformation in two-dimensional covalent organic frameworks under compressive loading. *Phys. Chem. Chem. Phys.* **2018**, *20*, 29462−29471.
(66) Lin, S.; Li, W.; Li, S.; Zhang, X.; Chen, Z.; Xu, Y.; Chen, Y.; Pei, Y. High thermoelectric performance of Ag9GaSe6 enabled by low cutoff frequency of acoustic phonons. *Joule* **2017**, *1*, 816−830.
(67) Luu, S. D. N.; Supka, A. R.; Nguyen, V. H.; Vo, D.-V. N.; Hung, N. T.; Wojciechowski, K. T.; Fornari, M.; Vaqueiro, P. Origin of low thermal conductivity in In4Se3. *ACS Appl. Energy Mater.* **2020**, *3*, 12549−12556.
(68) Parrinello, M.; Rahman, A. Strain fluctuations and elastic constants. *J. Chem. Phys.* **1982**, *76*, 2662−2666.
(69) Redfern, L. R.; Robison, L.; Wasson, M. C.; Goswami, S.; Lyu, J.; Islamoglu, T.; Chapman, K. W.; Farha, O. K. Porosity dependence of compression and lattice rigidity in metal-organic framework series. *J. Am. Chem. Soc.* **2019**, *141*, 4365−4371.

https://doi.org/10.1021/acs.jpcc.1c02767
J. Phys. Chem. C 2021, 125, 12991−13001